Article

Numerical Study of the Sports Car Aerodynamic Enhancements

Krzysztof Kurec (ID)

Micromechanics and Fotonics Institute, Warsaw University of Technology, Sw. A. Boboli 8, 02-525 Warsaw, Poland; krzysztof.kurec@pw.edu.pl

Abstract: This study was prepared to demonstrate how the aerodynamics of a sports car can be enhanced, emphasizing aerodynamic improvements, and utilizing small movable elements. All the presented results were obtained using the numerical simulations performed in ANSYS Fluent in steady-state conditions. It was investigated how the performance of a car equipped with the splitter and the rear wing could be improved. The benefits of a top-mounted wing configuration were presented compared to a bottom-mounted setup. A change to the top-mounting configuration enabled undisturbed flow around the suction side of the wing and a more favorable placement of the wing to the car body. In the given case, an 80% increase of downforce was achieved in the performance mode of the car setup and a 16% increase of drag in the air braking mode. A method of the front splitter active steering was presented, which enabled a change of the generated downforce using only a small element that enabled an instant change of 30% without the necessity of moving the whole splitter plate. The described modifications of the sports car not only improved its aerodynamic properties but also enabled the means to accommodate it with an active aerodynamic system that would allow a quick adaptation to the current driving conditions.

Keywords: sports cars aerodynamics; active aerodynamics; flow control; front wing; rear wing

1. Introduction

Sports cars need to stand out with their design, as well as their performance. Sometimes these two features overrule each other. A car with outstanding aerodynamic properties, such as a high downforce and an extremely low drag, might not appeal to a broad spectrum of car enthusiasts due to its looks. This situation can also work the other way. A car appreciated for its design might have an underwhelming driving performance or even be dangerous to drive, such as the early version of the Audi TT, which had to be equipped with a rear spoiler, otherwise, this car might lose track while cornering. In such cases, the active aerodynamics can be utilized so that, while not needed, active elements can be kept within or under the car's body and be ejected when the aerodynamic properties of the car need to be enhanced. Typical aerodynamic devices, which usually are fixed in one place and do not change their position (with the most common exception being the rear wing), can be found in [1–3].

The most widely known active aerodynamic element on the front of a car is a deployable spoiler, as found on such cars as the Porsche 911 Turbo [4] or the Porsche 918 Spyder. A different approach to generating additional downforce on the front axle was implemented in the Mercedes-AMG GTR [5], which has an underbody equipped with an aerodynamic profile that can be deployed when the downforce on the front axis needs to be increased. However, only a few other examples of active aerodynamic elements can be found on the front of the car, which demonstrates how desirable it is to investigate the new means to modify the downforce generated on the front axle. One such example is the 2004 version of the Ford GT [6], which in its final version was equipped with a mechanism that enabled the reduction of downforce generated on the front splitter.

One of the papers that tackles the topic of car aerodynamics improvement includes [7], which focuses on the gurney flaps attached to the front wing of a Formula 1 car. This paper

demonstrated that by utilizing such a small element as a gurney flap, the downforce could be increased up to 24% with only a minimal drag increase, and it presented what flow interactions occurred between different car body parts by mounting a gurney flap.

In [8], drag and lift optimization of an in-house built sports car was performed, where the focus was put on each section of the car. In the front, elements such as the splitter, air curtains, and number plate positionings were investigated. Several designs of the car's sides were tested to ensure that the flow was directed smoothly from the front to the rear. Where the rear of the car was concerned, elements that were put under scrutiny included the roof curvature and height, rear wing shape, as well as ducts and vents.

In [9], corner braking was investigated using a Computational Fluid Dynamic solver combined with a Multibody Dynamic System, which meant that the authors could consider factors such as the speed and force required to move the rear wing.

A review of active aerodynamic systems for road vehicles can be found in [10,11]. It described how movable car elements could be utilized to influence car dynamics and the importance of control systems that had to be developed to use these aerodynamic devices. In [12], a case study was presented in which the active aerodynamics control system was designed and tested numerically, and [13] demonstrated lap time reduction for a vehicle equipped with an active aerodynamic system. Another article covering this topic was [14], which demonstrated how movable front and rear wings could improve driving performance. At the same time, [15] investigated utilizing aerodynamic surfaces to suppress vibrations caused by terrain irregularities.

One of the most recent academic papers on active aerodynamics included investigations of a Formula SAE car equipped with an airbrake consisting of a two aerofoil rear wing [16] or airbrake mounted on an Ahmed body [17]. An interesting experimental design with active aerodynamic devices was presented in [18].

The focus of this paper is put on the modifications of a particular sports car, with its unique properties, which on the one hand, can be beneficial, whereas others need to be addressed. Such problems do not occur while a simplified car geometry is investigated (as the Ahmed body) or when the investigated car geometry is strictly devoted to racing (as the Formula SAE cars) and its purpose is entirely focused on performance. Since the significant focus is on the car's looks and design, it is not the case in the experimental design that aerodynamics is the focal point but must be compromised and adjusted. Therefore, that is why this paper may be helpful when an existing car design needs its aerodynamic properties adjusted.

This paper presents practical implications on an actual car model, the polish supercar Arrinera Hussarya. Key elements of the presented investigations include the advantages of changing the rear wing's mounting setup from the bottom to the top and the proposed design of an active front splitter. Modifications of the front of the car are presented, which can be utilized to modify the car's aerodynamic balance smoothly. The presented active splitter, with a plate on its trailing edge, can block the flow over it and enable the possibility to instantly suppress the aerodynamic downforce that the splitter generates. This paper also presents how to maintain a favorable car balance while active elements are introduced at the rear and the front of the car. Several recent papers investigated various aspects of aerodynamic modifications on the Arrinera Hussarya. In [19], the focus was put on the car during its cornering, where a particular aerodynamic setup of a rear wing and spoiler was investigated with different angles of attack and how the handling properties could be improved while cornering. In [20], a car with an inflatable splitter was investigated, and the results for different pitch angles were included.

This article focuses on active aerodynamics that improved the car's properties on its front and rear. On the front, it was studied how a movable element could interact with the splitter. Another investigated factor was the influence of the air intakes located at the front. On the car's rear, it was presented how the flow around the wing could be improved. It was completed for two modes of rear wing operation when it was set for maximum performance (increasing downforce with only moderate drag increase) and for braking

(to obtain maximum drag increase). Two mounting configurations of the rear wing were compared. The rear wing was mounted from its bottom and its top side. Mounting from the top is usually associated with a swan neck wing mount. A swan neck wing mount is used to improve the rear wing's performance since the flow on the suction side of the wing is not disturbed, which significantly improves the efficiency. An investigation of such a design can be found in [21,22]. Mounting from the top has one more advantage related to the steering mechanism. A bottom-mounted wing could be retracted within the car body by a servomechanism by moving it up and down. An example of such a design is in the Porsche 918 Spyder [23]. In contrast, a top-mounted wing enables a mechanism that uses rotational joints; this way, there is more freedom for the wing to be positioned in a more favorable position. This kind of design was introduced in the Koenigsegg Regera, and the flow properties of this aerodynamic setup could be found in [24].

The novelty of this article was the analysis of how a top-mounted retractable wing could improve car aerodynamic properties over the bottom-mounted one by considering how different mounting setups could improve the location of the rear wing with regard to the car body while it is deployed. The bottom-mounted retractable wing had more limitations in which the wing could be moved away from the car body. The other important part of this article was a proposed mechanism that allowed rapid change in the downforce generated by the splitter by incorporating a rotatable plate at the trailing edge of the splitter plate. Both of the mentioned features could be incorporated into an active aerodynamic system of a car that would allow for rapid adjustments to the current road conditions, which makes it interesting to follow their development.

2. Materials and Methods

This study was prepared through computational fluid dynamics in the ANSYS Fluent [25] software on the Fujitsu Intel Xeon workstation equipped with 24 GB RAM.

The initial geometrical configuration that the presented investigation started with was the original geometry of the Arrinera Hussarya, which was investigated during the "Active system of car body oscillation damping" project. The car was equipped with an active rear wing, which could be ejected and had the option to adjust its angle of attack. In the performance mode, the rear wing was inclined at an angle of attack equal to $10°$, whereas in braking mode, it tilted forward to the maximum possible angle equal to $55°$. On the front, there were no active devices. One of the aims of the presented research was to propose changes that would enhance the performance of this car.

In Figure 1a, the computational domain with mesh on the symmetry plane is presented, whereas, in Figure 1b, the close-up of the car body can be seen. The computational domain's length in front of the car was equal to two car lengths, while behind it was equal to five car lengths. It stretched to the side and the top by two lengths of the car body. The car's frontal area was equal to 1% of the domain's entire cross-section to prevent the outer walls of the domain from influencing the results.

The polyhedral mesh was generated with six layers of prism elements on the car body and all the attached elements, with a growth rate set to 1.2. The mesh in the boundary layer is presented in Figure 1c. The average y+ value on all the car elements was equal to 84, and on the wing with its mounting, the average y+ value was equal to 38 (the y+ contours are presented in Figure 1d). It could be seen in Figure 1a that two zones of refinement were set around the car to make sure that the flow in the wake of the car model was resolved correctly and to avoid too rapid of a transition between the small size elements on the car body and the larger ones in the far-field.

Numerical simulations were performed utilizing the pressure-based solver and the steady-state Reynolds-averaged Navier-Stokes (RANS) equations with the Shear-Stress Transport (SST) k-ω [26] turbulence model. Pressure-velocity coupling was performed using the SIMPLE scheme, and the gradients were calculated using the Least Square Cell Based method. The governing equations of the utilized numerical model and the

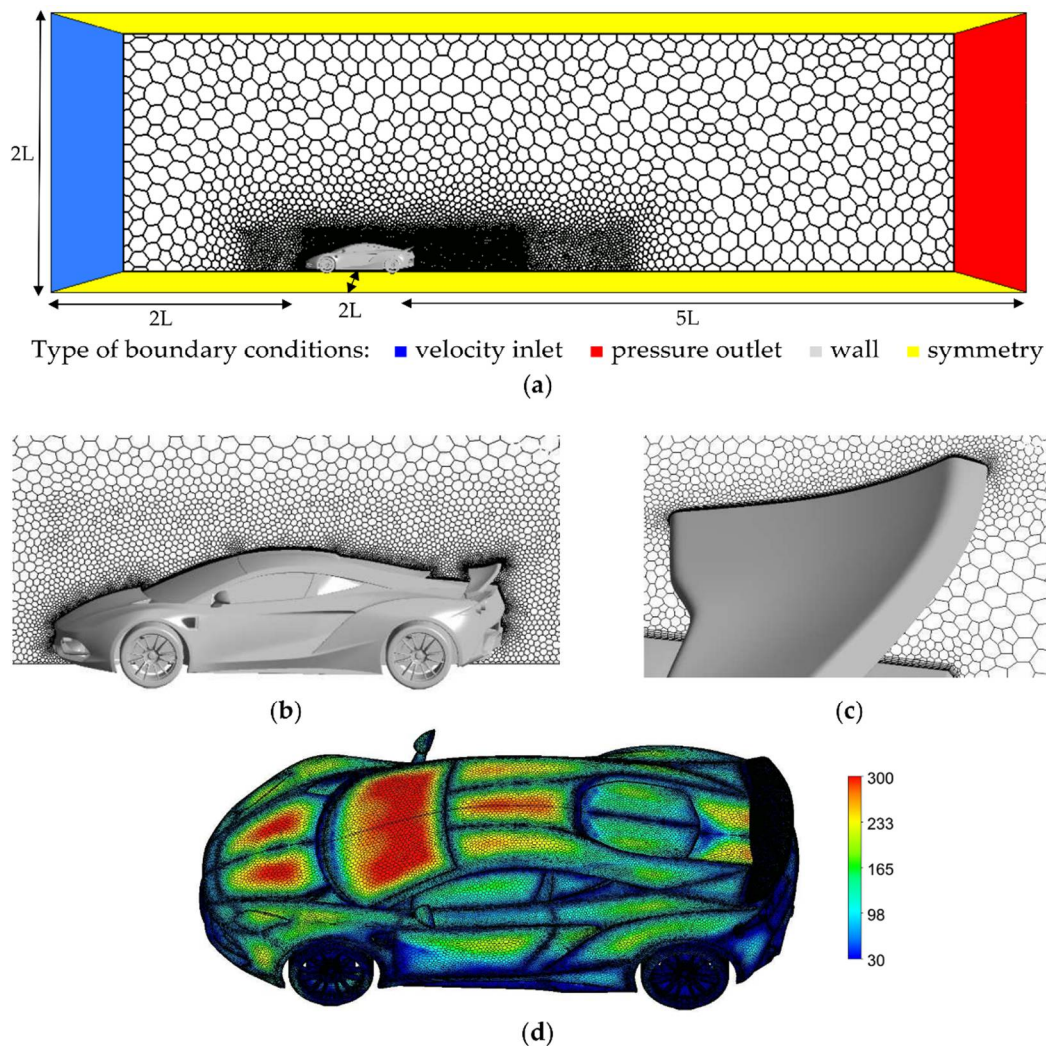mathematical expressions of the boundary conditions used can be found in ANSYS Fluent Theory Guide [25].

Figure 1. (**a**) Computational domain with mesh at the symmetry plane (letter L is the length of the car); (**b**) close-up on the mesh around the car; (**c**) the rear wing; (**d**) y+ values on the car body with superimposed surface mesh edges.

Half of the car's geometry was used in simulations since only the head-on flow was investigated, and the aerodynamic setup of the car was symmetric in all the studied cases. Flow inlet to the computational domain was set as velocity inlet, with the velocity magnitude equal to 60 m/s. Assumed parameters of turbulence on the inlet boundary conditions were turbulent intensity equal to 5% and viscosity ratio equal to 10. The flow outlet was set as a pressure outlet condition. Outer faces of the domain and the ground were set to the symmetry condition so that no boundary layer could build up on these surfaces. Wheels were modeled as stationary without rotation.

Validation of the numerical model is presented in [19], using data obtained during tests in the MIRA wind tunnel. The 1:1 scale car model was investigated with fixed wheels, while standing on the stationary ground at a flow velocity equal to 35 m/s. The car geometry investigated in the MIRA wind tunnel was the GT version of the Arrinera Hussarya, which differed from the road version by utilizing a fixed rear wing (it can be retracted in the road version), splitter, and an additional air intake on the roof. It was reported that the absolute percentage error of the drag coefficient was equal to 3.8%, and the absolute percentage

error of the lift coefficient was equal to 6.5%, thus proving that the employed numerical model was good enough to predict the aerodynamic properties of this car. The value of the absolute percentage error was calculated according to the following formulas:

$$Cl_{error} = 100\% \cdot |(Cl_{MIRA} - Cl_{CFD})/(Cl_{MIRA})| \tag{1}$$

$$Cd_{error} = 100\% \cdot |(Cd_{MIRA} - Cd_{CFD})/(Cd_{MIRA})| \tag{2}$$

where *Cl* refers to the lift coefficient and Cd to the drag coefficient.

The modifications to the aerodynamic properties presented in this paper focused on significant aerodynamic changes, where the chosen numerical setup was adequate to predict. If more subtle changes to the flow field were of the main interest, more complex numerical methods should be applied, as discussed in [27]. All the presented results were obtained in a steady state, meaning they did not include any instantaneous phenomena that might occur in a real-life scenario. When active aerodynamic elements were slowly adjusted, it could be assumed that the quasi-static process was taking place. However, additional forces could be observed when rapid movements occurred, or a significant change in orientation, which was particularly important during braking [28].

3. Results

3.1. Grid Dependency Study

In order to ensure that the simulations' results were grid independent, the results on three different meshes were compared, consisting of 950,195, 2,333,982, and 4,597,031 polyhedral cells. The comparison of the aerodynamic coefficients is presented in Figure 2, and it can be seen that with an increased number of cells, the drag and lift force coefficient values remained at a constant level, proving that the 4,597,031 elements mesh could be used in further investigations.
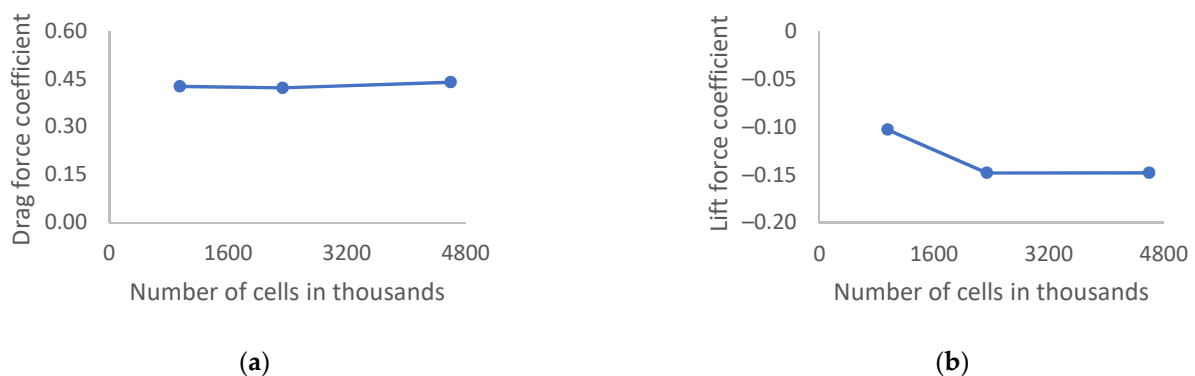

(**a**)   (**b**)

Figure 2. Values of (**a**) drag force coefficient and (**b**) lift force coefficient for different grid sizes used in calculations.

3.2. Rear Wing Improvements

The most widely used mechanism to change the position and angle of attack of a rear wing mounted on sports cars was a servomechanism attached to the bottom side of the wing (as in the left column of Figure 3a). It was used to push the wing up, deployed from the car's body, and changed its operation mode between maximum performance (an increase of downforce) and braking (maximum increase of drag). However, utilizing this kind of mechanism has several drawbacks. Mounting from the bottom of the airfoil disturbed the flow in the region where the wing generated the highest downforce. It caused the mechanism to transfer loads the least favorably through compression, which could lead to buckling and made this mechanism more prone to getting stuck.
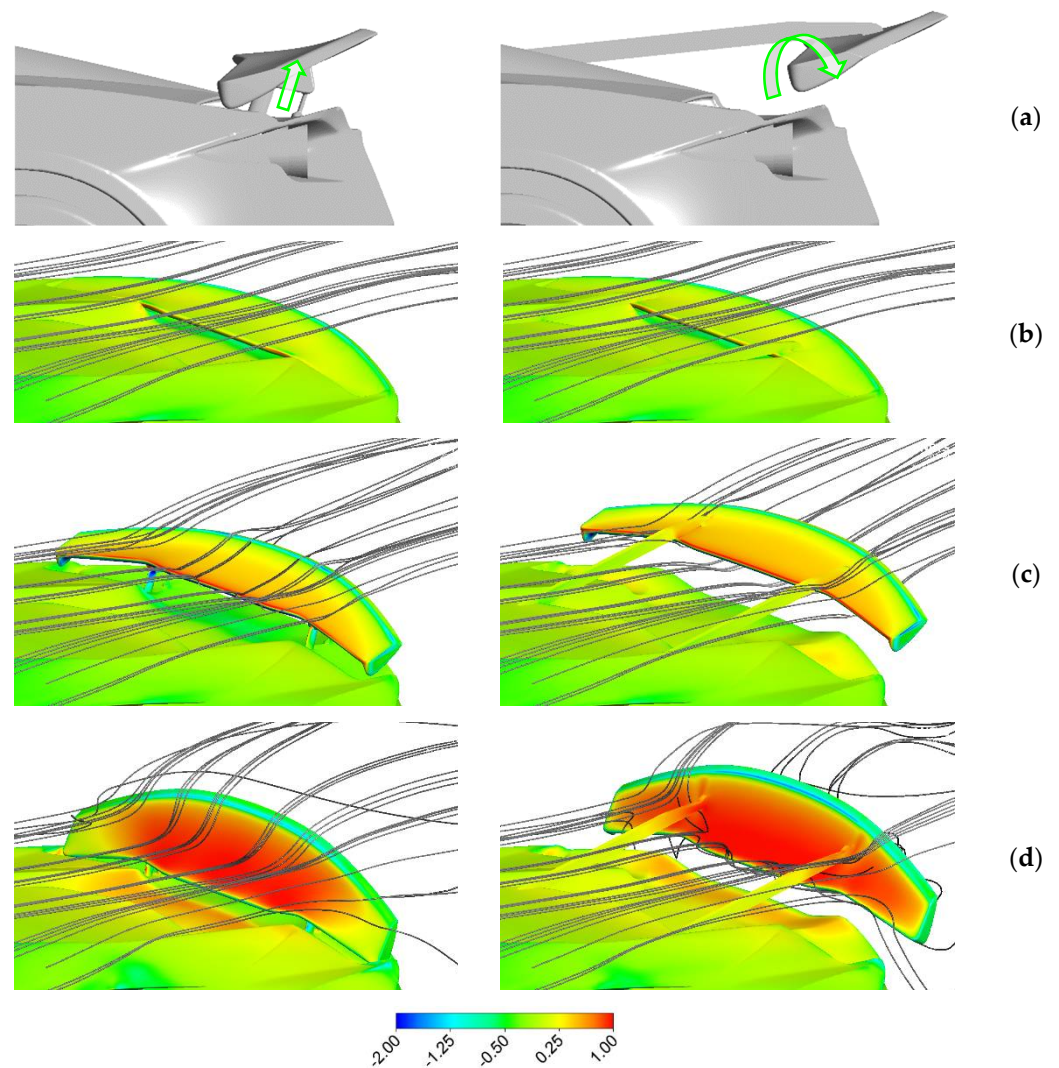
Figure 3. (**a**) Geometry of the bottom-mounting (**left** column) and top-mounting (**right** column), with arrows depicting the movement of the wing when it is ejected and contours of pressure coefficient on the car's body with superimposed path lines: (**b**) wing retracted; (**c**) maximum downforce; (**d**) braking.

The airflow on the low-pressure side of the wing was highly susceptible to flow detachment caused by disturbances from the pylons supporting the inverted wing. In order to avoid this phenomenon, attempts were made to mount the wings on the pressure side. For example, in the case of the Koenigsegg cars, the inverted rear wing was mounted on horizontal pylons extending from the body (as in the right column of Figure 3a). However, this required more complex pylon mechanics (implementation of pylon extension and upward rotation). Where the transfer of loads was concerned, this type of wing mounting allowed the wing to be attached on the boost side, and during aerodynamic braking, the aerodynamic drag forces were transferred along the pylons. Alternatively, the aerodynamic downforce caused the pylons to bend.

A mechanism mounted from the top and bottom was compared, starting from the case with the rear wing retracted to the car body. As seen in Table 1, Figures 3b and 4a,b, the results were the same due to minor differences in geometry. In the top-mounted version, the pylons supporting the rear wing were located over the car body. Apart from that, both of the investigated geometries were the same.

Table 1. Aerodynamic coefficients for the bottom and top rear wing mounting.

Case	Bottom-Mounted		Top-Mounted	
	Drag Coefficient	Lift Coefficient	Drag Coefficient	Lift Coefficient
Retracted	0.412	0.023	0.408	0.019
Performance mode	0.440	−0.148	0.470	−0.270
Braking mode	0.606	−0.410	0.623	−0.374

The second case (Figure 3c) was for the wing set to the Performance mode, in which the aerodynamic downforce was increased, only with a minimal drag increase. The wing was moved up for the setup with the control mechanism attached to its bottom and inclined at the attack angle equal to 10°. In contrast, the setup with the top-mounting enabled moving the wing higher and to the rear, so it was moved further away from the car body. Whereas in both setups, the angle of attack was kept the same.

This less significant interaction between the wing and the car body significantly improved the generated downforce coefficient, with the gain equal to 0.12 (Table 1). In Figure 3c, it could be seen that for the top-mounted configuration, pressure on the trailing part of the car body was higher, which occurred from the fact that for the bottom-mounted configuration, the low-pressure zone from the suction side of the wing reached the car body. It was the primary source of downforce difference between both configurations. The other one was that in the top-mounted configuration, the rear wing diverted the flow more upwards, in comparison to the bottom-mounted one, which could be seen in the left column of Figure 4c,d, which led to an improvement in the efficiency of the diffusor and decrease of the pressure on the rear end of the car underbody (right column in Figure 4c,d).

In the third case, a braking position was analyzed, with the wing set to the maximum angle of attack equal to 55° (Figure 3d), to obtain the maximum available drag force. The drag force generated in both setups was almost identical (Table 1). More downforce was obtained for the bottom-mounting. In this case, a location closer to the car body was more beneficial since it created a high-pressure zone that reached further towards the front of the car, which contributed to more downforce being generated on the top side of the car body (right column in Figure 4e,f). This phenomenon can be explained by the fact that in the top-mounted configuration, a gap was formed between the rear wing and the car body, leading to the flow "leaking" through that region (left column in Figure 4e,f).

In the case of top mounting, to obtain more downforce, it would be necessary to realize the pylon's downward rotation to reduce the clearance under the leading edge of the rotated wing, which is why the wing's braking position was further investigated in the next section.
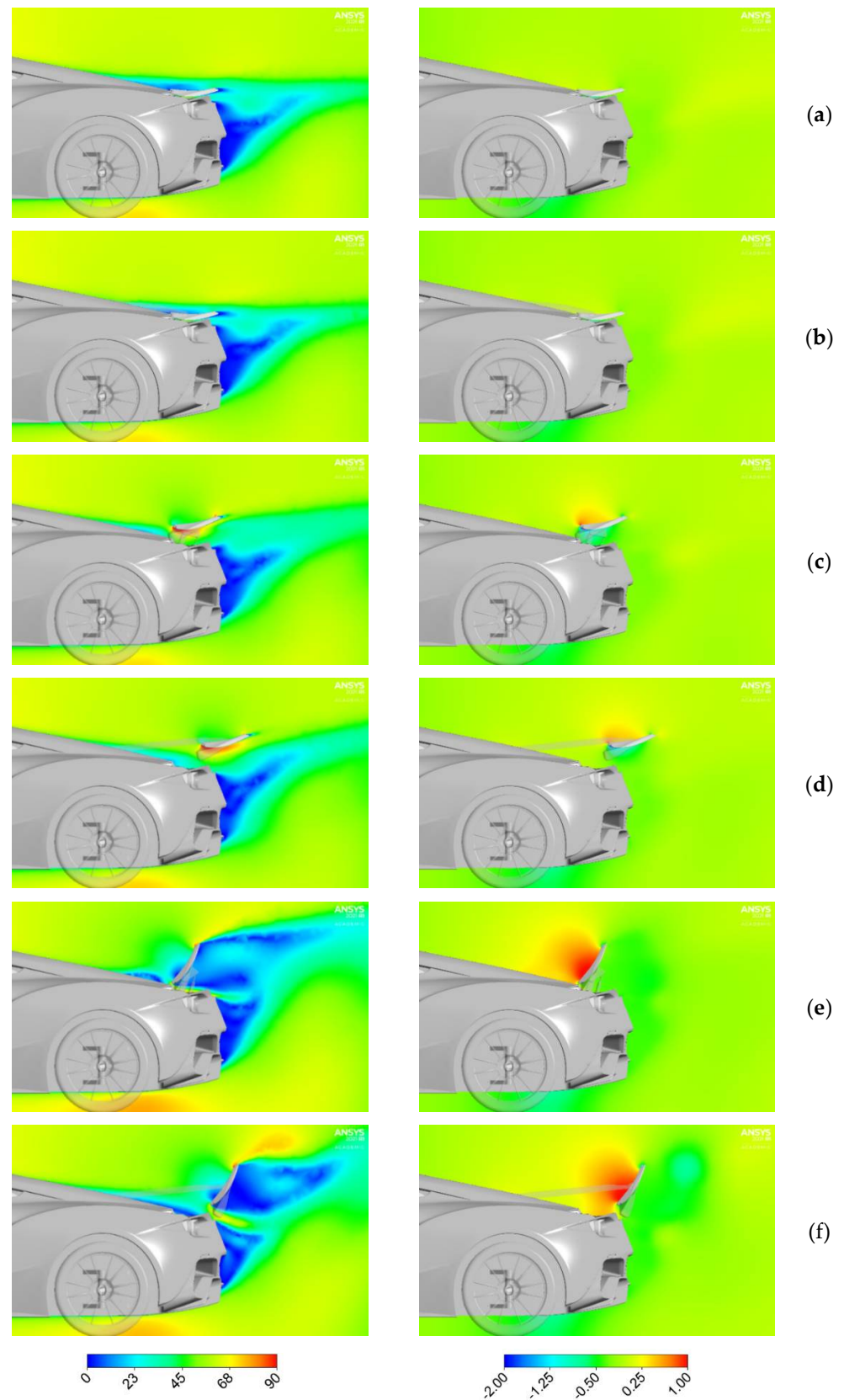
Figure 4. Contours of velocity (m/s) (**left** column) and pressure coefficient (**right** column) on the symmetry plane: (**a**) Wing retracted in the bottom-mounted configuration, and (**b**) top-mounted, (**c**) Performance mode—bottom-mounted, and (**d**) top-mounted, (**e**) Braking mode—bottom-mounted, and (**f**) top-mounted.

3.3. Top-Mounted Rear Wing Braking Improvements

The first attempt to improve the efficiency of the top-mounted rear wing in the braking position was to move it to a lower position (Figure 5b), as in the setup where it was mounted from the bottom while simultaneously keeping it at the exact horizontal location. This alone did not improve the generated aerodynamic coefficients (Table 2). Despite lowering the wing, there were gaps between the sides of the rear of the car and the wing. When the wing was mounted from the bottom, it was moved forward, so these gaps did not exist. When the rear of the car had a complicated shape, it may be impossible to match it perfectly with the wing's geometry so that no gaps would be present. It could be seen in the left column of Figure 6b that much less air was coming through the space between the wing and the car present in the symmetry plane, but simultaneously, the pressure increase that the rear wing posed was significantly smaller (Figure 5b, and right column of Figure 6b), which could be explained by the fact that when the wing was higher, it reached further to the zone of the airflow less disturbed by the car body.
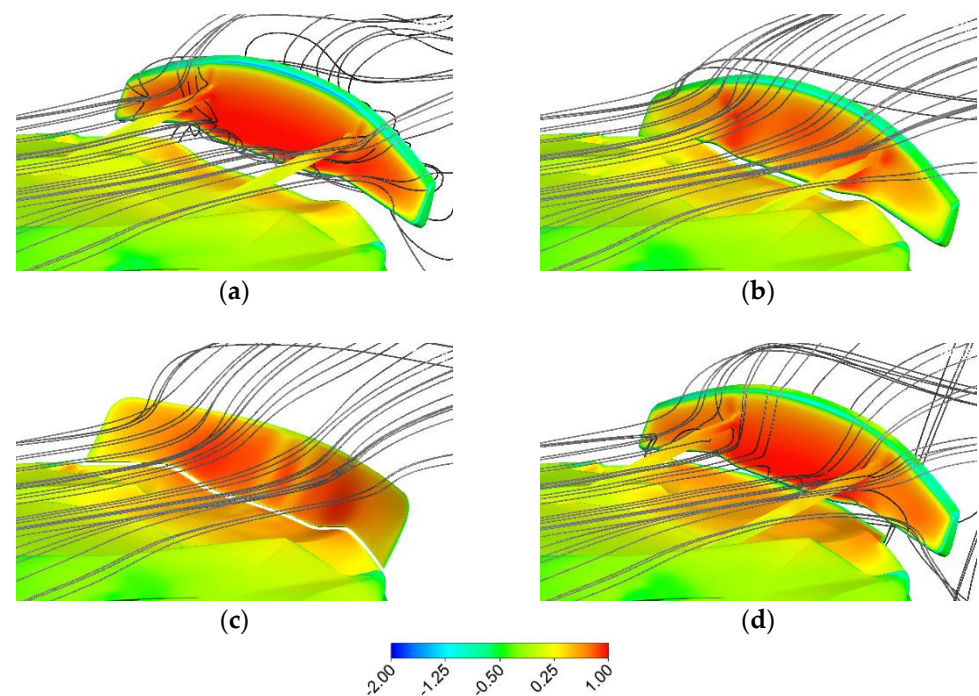

Figure 5. Contours of pressure coefficient on the car's body with superimposed pathlines: (**a**) Top-mounted (base case); (**b**) lowered; (**c**) fitted to the edge; (**d**) original position with spoiler.

Table 2. Aerodynamic coefficients for the rear wing in the braking mode.

Case	Drag Coefficient	Lift Coefficient
Top-mounted (base case)	0.623	−0.374
Lowered	0.581	−0.364
Fitted to the edge	0.634	−0.534
Original position with spoiler	0.721	−0.596

In order to check how the gaps mentioned above deteriorated the braking capabilities, the car's trailing edge was extruded to obtain a surface of the same area as the wing (Figure 5c). In this case, there was only a uniform gap between the car and the wing equal to 12 mm. It can be seen in Table 2 that values of drag and downforce were improved, whereas, in the case of the lift the increase was equal to 61% in comparison to the previous setup when the wing was lowered. In Figure 5c and the right column of Figure 6c, it can be seen that the pressure on the rear end of the car body and surface imitating the wing was

higher than in the previous case, and it was more uniform on the sides of the car as well as on the introduced surface. On the downside, it could be observed (left column of Figure 6c) that the flow "leaking" through the small gaps between the wing and the car body was sticking to the car body and was directed downwards at the back of the car, which could be presumed to lead to the lowering of the generated downforce.
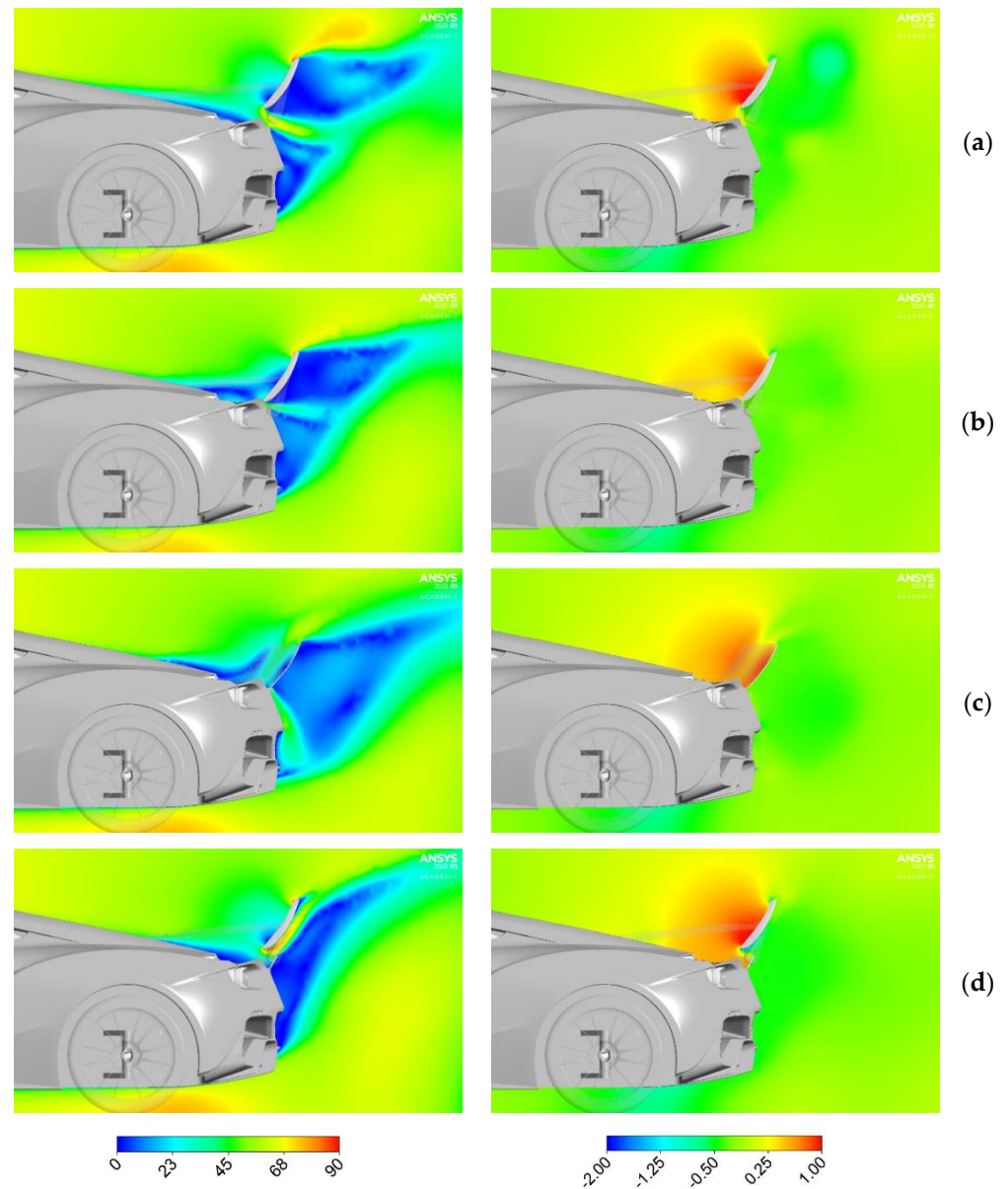

Figure 6. Contours of velocity (m/s) (**left** column) and pressure coefficient (**right** column) on the symmetry plane: (**a**) Top-mounted (base case); (**b**) lowered; (**c**) fitted to the edge; and (**d**) original position with spoiler.

The wing's geometry in the shape of the surface introduced in the previous paragraph would not allow the wing to fit the car body when retracted. It would also be tough to slide a rear wing of this size from within the car body. However, it would be possible to mount a small spoiler on the car's rear that could be ejected (Figure 5d). It can be seen in Table 2 that this modification improved the aerodynamic coefficients even above those obtained for the surface that perfectly fit the trailing edge of the car. In this configuration, the wing was moved back to the height it was mounted in the base configuration. It would be more feasible if the wing's location were not modified and kept the same in both the

braking and performance modes. This modification brought further improvements, and this configuration turned out to be the best of the studied ones. In Figure 5d and the right column of Figure 6d, it can be seen that the zone of high pressure induced by the flow was the most significant compared to all other cases. In the left column of Figure 6d, it can also be seen how well, compared to other cases, the flow from the car's underside was directed upwards, further increasing the downforce generated in that region. A similar rear spoiler that enhanced the performance of the rear wing could be found on the Bugatti Veyron, a car with one of the most powerful aerodynamic brakes [29]. In the case of the Bugatti Veyron, the spoiler prevented the flow from staying attached to the smooth rear end of the car body and directed it towards the wing.

In the final and most favorable case studied, it could be seen (left column of Figure 6d) that the flow attached to the airfoil, thanks to being diverted by the spoiler, which occurred even though the attack angle of the wing was significant. Attaching the flow to the suction side of the wing might recall the active aerodynamic system utilized in the Lamborghini Huracán Performante, as described in [30,31]. Flow stayed attached to the wing via flow discharge from the wing itself. However, the wing was at a more moderated angle of attack to aid the performance. For a higher angle of attack, such as in this study, a spoiler must have influenced the flow's direction.

3.4. Active Splitter

A splitter is one of the most commonly used aerodynamic devices mounted at the car's front. Below, Figure 7 presents some of the configurations that enabled modifying its properties. The first studied configuration (Figure 7b) was of a splitter mounted to the car's underbody without protruding out in front of the car body. This splitter plate could be rotated and moved forward (as depicted in Figures 7c and 8c) if mounted on a hinge. With the inclusion of the splitter, a significant increase in downforce compared to the base case could be observed. This increase equaled 75% (Table 3) when the splitter was retracted and 63% when deployed. When the splitter was deployed, the air could flow over it, and the pressure on its top side was lower than when it was retracted (Figure 7b,c). This phenomenon entailed a smaller detachment zone on its underside, which lowered the pressure in that region. Thus, the deployed version of the described solver generated a lower downforce than the retracted one, even though the deployed version protruded in front of the car.
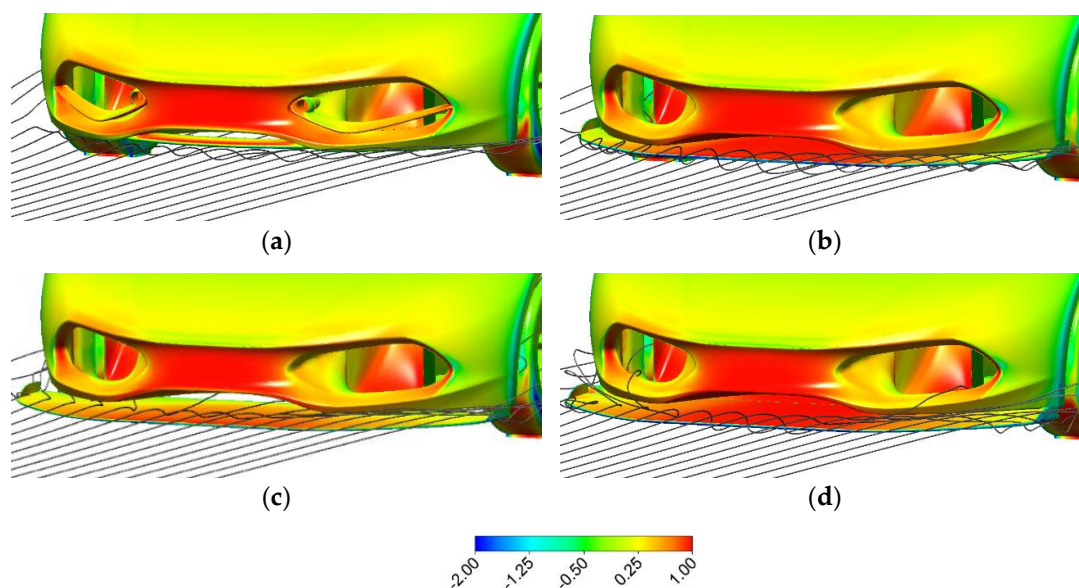

Figure 7. Contours of pressure coefficient on the car's body with superimposed pathlines: (**a**) Base geometry; (**b**) retracted spoiler; (**c**) deployed spoiler; and (**d**) deployed spoiler with a vertical plate.
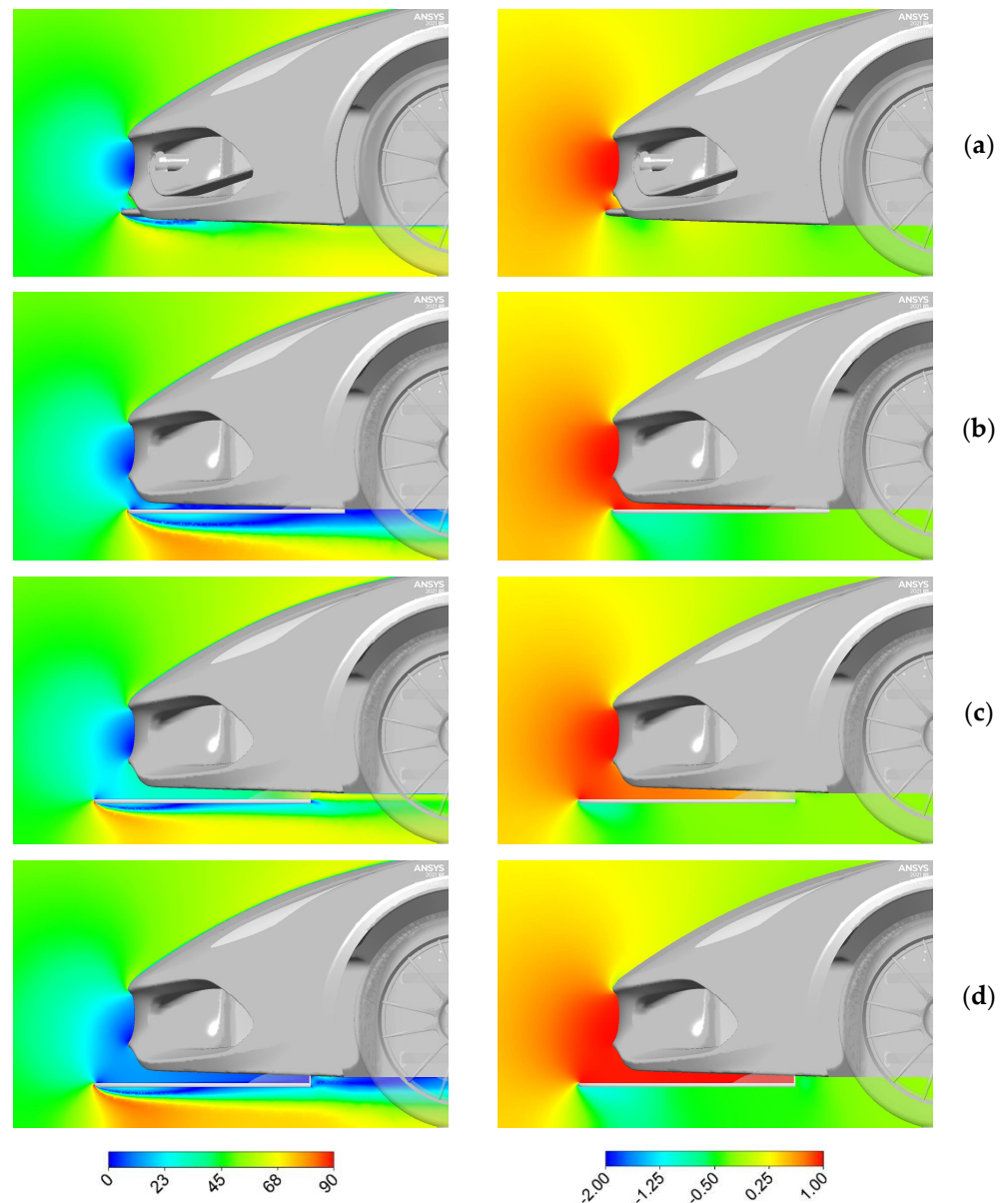
Figure 8. Contours of velocity (m/s) (**left** column) and pressure coefficient (**right** column) on the symmetry plane: (**a**) Base case geometry; (**b**) retracted splitter: (**c**) deployed splitter: (**d**) deployed splitter with a vertical plate.

Table 3. Aerodynamic coefficients with the active spoiler.

Case	Drag Coefficient	Lift Coefficient
Base geometry	0.470	−0.270
Retracted spoiler	0.466	−0.472
Deployed spoiler	0.476	−0.441
Deployed spoiler with vertical plate	0.498	−0.574

The utilized splitter was a large element, with its movement restricted in time and significant energy needed to be supplied to the control mechanism. Thus, it was equipped with a small plate at its trailing edge (Figures 7d and 8d), which could either block the flow when placed horizontally or let it go when inclined in a horizontal direction. When the plate blocked the flow over the splitter, an increase in the flow's velocity magnitude under

it could be observed, which further contributed to a decrease in pressure in that region (Figure 8d) and an increase in downforce (Table 3).

In road conditions, the described way of reducing the downforce could be utilized when there was too much downforce on the front axle, and the car balance had to be moved to its rear. Another example included when the car moved at a remarkably high speed, and the overall downforce needed to be reduced to ease the force transferred by the car's suspension. That was why the proposed configuration of the splitter could be utilized in an active aerodynamic system, providing a quick response to the current road conditions. The described splitter with a plate at its trailing edge was inspired by the patent [32] presenting a vehicle body vibration suppression system during fast driving. Since the plate could be rotated at almost any given rotational velocity, it could generate aerodynamic forces on the splitter and the car body to counter the car body's oscillations. Therefore, this was one more example of how this design could improve driving performance and safety. The spoiler mounted behind the rear wing, described in the previous chapter, could be utilized as a part of this system, but it would be more feasible if it were not curved, enabling it to rotate.

In the computational setup used, the ground boundary condition was set to symmetry, which meant zero-shear slip on this surface. Due to the proximity of the splitter to the ground, more accurate results would be obtained using a moving wall condition. However, it should be accompanied by the inclusion of prism elements built up on this surface, further increasing the total number of elements in the mesh and thus extending the time of computations. In order to evaluate how the chosen model setup affected the results, a comparison of results with and without the boundary layer effect is presented in Appendix A. According to the results presented in Appendix A, in the investigated case, only minor discrepancies occurred when the boundary layer on the ground was resolved, with the most significant difference being a further increase in the car's downforce by 2.3%.

3.5. Influence of Channels to the Wheel Chamber and over the Mask

The investigated car body model was equipped with two sets of air intakes at its front. The channel closer to the car's side (the green surface in Figure 9) supplied the air to the wheel chamber, and its primary function was to provide fresh air to cool the brakes. This channel could be either opened or closed, depending on the temperature of the brakes. The second channel, near the car's center (the yellow surface in Figure 9), was also used as the cooling air intake to support the engine cooling. The base case with open channels included the splitter described in the previous chapter. Whether the channels were opened or closed, the air stagnation forming at the front of the car changed, and that was why it was investigated how much influence it would have on the generated downforce and whether it would have as significant an impact as the plate at the trailing of the splitter investigated in the previous chapter.
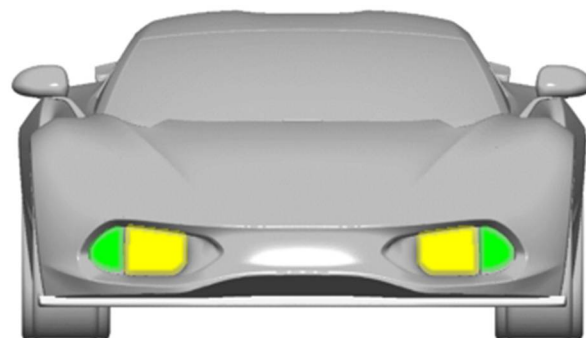

Figure 9. Front view of the car with the two sets of flow inlets at the front, inlets to the wheel chamber (green), and inlets leading the flow over the mask (yellow).

These channels could be opened and closed with a shutter mechanism, as described in [33]. This device controlled air intake to the heat exchanger and blocked the flow to decrease the car's drag when needed. In the investigated geometry, no shutters were included, thus, the opened intakes represented a case when the shutters would be inclined at a 90° angle to let the flow enter the channels. Closed intakes represented a case with shutters inclined at a 0° angle, which entirely blocked the entrance to the channels.

When both channels were blocked (Figure 10b), the flow accelerated and moved faster towards the side or top of the hood, which decreased the pressure pushing the car body down, and the downforce was reduced (Table 4), at the same time, the drag was reduced since the flow did not pass through the cooling passages.
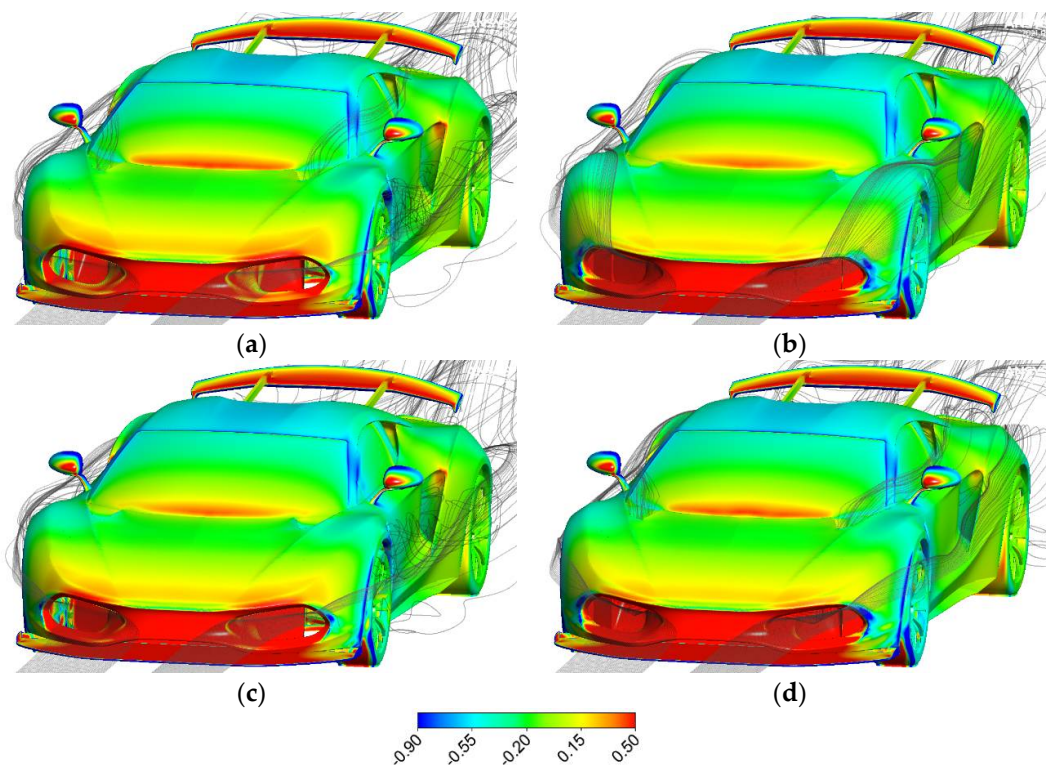

Figure 10. Contours of the pressure coefficient on the car's body with superimposed pathlines: (**a**) Both inlets opened, (**b**) both inlets closed, (**c**) inward inlet blocked, (**d**) outward inlet blocked.

Table 4. Aerodynamic coefficients for different air intakes configurations.

Case	Drag Coefficient	Lift Coefficient
Both inlets opened	0.498	−0.574
Both inlets closed	0.486	−0.515
Inward inlet blocked	0.492	−0.586
Outward inlet blocked	0.485	−0.502

Interestingly, the channel providing air to the wheel chamber (Figure 10c) improved the downforce when it was opened (Table 4), which was possible since there was an outlet from the wheel chamber on the side of the car, which prevented the additional flow coming through the wheel chamber to increase pressure on the wheel chamber walls, which would generate lift.

When both channels were blocked, it could be seen in Figure 10b that the air that would flow through the wheel chamber instead attached to the car body over the wheel decreased pressure in that region, reducing the downforce. It must be stressed that there were no heat exchangers included in either of the channels, which should have further

increased the drag when the flow entered them. Therefore, it would be expected that in a real-life case, the closing of these channels should significantly reduce drag. Nevertheless, when the outer inlet was closed (Figure 10d), the drag was reduced with the limited flow in the vicinity of the wheel and the brake disc.

In the investigated case, the cooling channels were blocked a couple of centimeters behind the front fender, where their cross-section was rectangular. The total area of the channel's cross-section that was cut off was almost six times larger than the area of the plate mounted on the trailing edge of the splitter. As mentioned earlier, a shutter mechanism must be introduced to close these channels, whereas in the second case, only a single plate had to be rotated to a position parallel to the splitter. Where the maximum difference in lift coefficient that was observed was significant (equal to 0.084), it must be emphasized that the results presented in the previous section showed a change of up to 0.133 that was generated by the change of position of a much smaller small plate behind the splitter. This is a further example of a significant difference a well-placed active aerodynamic element can make.

3.6. Car Balance

The focus of this paper was on improvements or modifications of each particular active aerodynamic element. However, it is necessary to present how the introduced modifications influenced the car balance, which is essential to driving stability and safety. The data presented in Table 5 refers to the key cases presented in previous paragraphs. The first case was without any active elements in which the lift was generated on the car body, which meant that additional elements must be activated to increase the downforce.

Table 5. Load distribution of the lift coefficient (Cl) for previously presented results.

Case No.	Case Name	Activated Elements	Cl Front	Cl Rear
1	All elements retracted	none	0.046	−0.027
2	Performance mode	wing	0.105	−0.375
3	Retracted spoiler	wing + splitter	−0.114	−0.358
4	Deployed spoiler	wing + splitter	−0.138	−0.303
5	Deployed spoiler with vertical plate	wing + splitter	−0.305	−0.269
6	Braking mode	wing	0.130	−0.726

The second case was for the activated rear wing at an angle equal to $10°$. The overall downforce was increased. However, this additional force was generated on the wing mounted right at the car's rear. Due to this, the downforce on the rear axle was increased but at the cost of a decrease on the front axle. Thus, active elements also need to be introduced on the front.

With the splitter introduced at the front, the downforce on the front axle was increased even when the splitter was retracted. Deployment of the splitter brought further improvement on the front axle, whereas further improvement could be observed when the plate on its trailing edge was activated. By utilizing this plate, the car's balance could be tuned by enabling a feasible increase of downforce on the front axle. In each case, the rear wing was kept at the same inclination angle, but with adjustments to its angle of attack, the load on the rear could be modified, which meant that the presented active aerodynamic elements had the potential to generate a high overall downforce and maintain a favorable distribution on the front and rear axle.

The last case in Table 5 refers to the configuration with the rear wing set to the braking position. The wing not only generated drag, which could be utilized to generate forces that directly slowed the car down, but also increased downforce. As can be seen in Table 5, the

increase of downforce on the rear axle completely disturbed the car's balance, meaning that the presented configuration could only be utilized while driving in a straight line, whereas while driving on a curve its use might be dangerous due to a sudden shift of downforce. An additional active element might be introduced on the front, such as the splitter, from the other cases to solve this problem. An alternative approach could involve mounting the wing further upfront on the car body. Therefore, the forces generated on the wing would not be applied right at the car's rear after activation. Such a case was investigated in [34]. One additional way to solve the balance shift was presented in [35], where active elements were mounted on the whole car body, preventing the additional downforce from generating in one location.

In order to put the results presented in Table 5 into a broader context, data provided for cars equipped with active aerodynamic devices were put in Table 6. The complete data can be found for the Porsche 911 Turbo and its three driving modes. The other two examples were for the Bugatti Chiron and Veyron 16.4 Sport in their "Handling" mode, which was equivalent to Porsche's "Performance" mode. As can be seen, when comparing this data with Table 5, the active aerodynamic devices on the Arrinera Hussarya provided a very respectable value of downforce and allowed a favorable car balance.

Table 6. Load distribution of the lift coefficient (Cl) for different sports cars.

Car	Driving Mode	Cl Front	Cl Rear
	Start	0.06	−0.01
Porsche 911 Turbo [4]	Speed	0.02	−0.03
	Performance	−0.05	−0.10
Bugatti Chiron [36]	Handling	−0.09	−0.26
Bugatti Veyron 16.4 Sport [29]	Handling	−0.11	−0.15

4. Conclusions

It was presented in this article how only minor modifications could change the aerodynamic properties of a car. While considering the rear wing setup, it was presented how the downforce can be increased by 80% for the maximum performance mode just by changing the mounting method, which enabled it to move off the wing into a more advantageous position. In the braking mode, the downforce increased to 62%, and the drag increased by 16%, but this time the change was posed only by adding a small plate below the wing.

Changes in aerodynamic coefficients for the different plate's orientations on the trailing edge of the splitter plated were smaller than in the case of the rear wing, but for the case where they were the most significant, the change of the downforce coefficient reached up to 30%, which was still a large change, considering how small the element that posed that change and that the downforce coefficient increased by 0.13.

The results presented in this article further emphasize the influence that the active aerodynamic elements can have on the aerodynamic properties of a car and, at the same time, show that significant changes can be obtained with the use of small movable elements. The proposed modifications of the car aerodynamic setup have a high potential to be incorporated into an active aerodynamic system that would allow rapid changes in the aerodynamic forces generated on the car body and its additional elements, such as the rear wing and front splitter, as well as to obtain the most favorable car balance for the current driving conditions.

Data Availability Statement: Data is contained within the article.

Conflicts of Interest: The authors declare no conflict of interest.

Appendix A

Comparison of results without and with boundary layer on the ground. An additional case was computed for comparison to show how the boundary layer forming on the ground under the splitter influences the results. The boundary condition type of the surface representing the ground was changed to the wall boundary condition with the moving ground option, where its velocity was equal to the velocity on the inlet. Apart from that change, the mesh was modified to include six layers of prism elements on this surface. While looking at the results presented in Table A1 and Figure A1, it could be concluded that in the investigated case, the boundary layer forming under the car influenced the results only in a minor way, with the lift coefficient of the car being decreased by 2.3% and only minor differences presented in the contours of velocity and pressure coefficient.

Table A1. Comparison of aerodynamic coefficients with and without boundary layer forming on the ground.

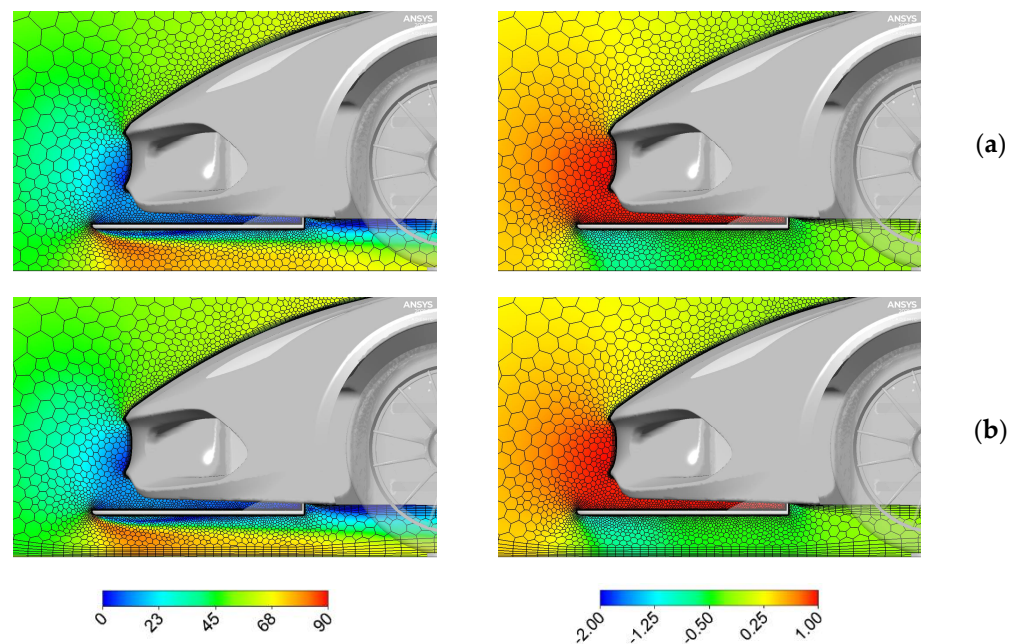| Case	Drag Coefficient	Lift Coefficient
Results from paragraph 3.4 without boundary layer	0.498	−0.574
Boundary layer effects on the ground	0.496	−0.587
Absolute percentage error	0.4%	2.3%

Figure A1. Contours of velocity (m/s) (**left** column) and pressure coefficient (**right** column) on the symmetry plane with superimposed mesh edges: (**a**) Results from paragraph 3.4 without boundary layer; (**b**) Results including boundary layer effects on the ground.

References

1. Katz, J. *Race Car Aerodynamics: Designing for Speed*, 2nd ed.; Bentley (Robert) Inc.: Cambridge, UK, 1996; ISBN 0837601428.
2. Schütz, T. (Ed.) *Hucho—Aerodynamik des Automobils*; Springer Vieweg: Wiesbaden, Germany, 2013; ISBN 978-3-8348-1919-2.
3. McBeath, S. *Competition Car Aerodynamics*, 3rd ed.; Veloce Publishing Ltd.: Poundbury, UK, 2015; ISBN 1845847768.
4. Meder, J.; Wiegand, T.; Pfadenhauer, M. Adaptive aerodynamics of the new Porsche 911 Turbo. *ATZ Worldw.* **2014**, *116*, 42–45. [CrossRef]
5. Estrada, G. Mercedes-AMG GTR: Aerodynamics for the Record. In *Progress in Vehicle Aerodynamics and Thermal Management*; Springer International Publishing: Cham, Switzerland, 2018; pp. 135–144.

6.   Harrison, K.E.; Landry, M.P.; Reichenbach, T.G. 2005 Ford GT—Vehicle aerodynamics—Updating a legend. In Proceedings of the SAE Technical Papers; SAE International: Warrendale, PA, USA, 2004.

7.   Basso, M.; Cravero, C.; Marsano, D. Aerodynamic Effect of the Gurney Flap on the Front Wing of a F1 Car and Flow Interactions with Car Components. *Energies* **2021**, *14*, 2059. [CrossRef]

8.   Dickison, M.; Ghaleeh, M.; Milady, S.; Subbakrishna, S.; Wen, L.T.; Al Qubeissi, M. Investigation into the aerodynamic performance of a concept sports car. *J. Appl. Fluid Mech.* **2020**, *13*, 583–601. [CrossRef]

9.   Broniszewski, J.; Piechna, J.R. Fluid-Structure Interaction Analysis of a Competitive Car during Brake-in-Turn Manoeuvre. *Energies* **2022**, *15*, 2917. [CrossRef]

10.   Piechna, J. A Review of Active Aerodynamic Systems for Road Vehicles. *Energies* **2021**, *14*, 7887. [CrossRef]

11.   Gao, W.; Kong, X.; Deng, Z.; Yu, W.; Wu, Y.; Luo, J. Review of state of the art in active aerodynamic control research for vehicles. In Proceedings of the Journal of Physics: Conference Series; IOP Publishing Ltd.: Bristol, UK, 2021; Volume 1985, p. 12040.

12.   Ferraris, A.; De Cupis, D.; Pinheiro, H.D.C.; Messana, A.; Sisca, L.; Airale, A.G.; Carello, M. Integrated Design and Control of Active Aerodynamic Features for High Performance Electric Vehicles. In Proceedings of the SAE Technical Papers; SAE International: Warrendale, PA, USA, 2021.

13.   De Buck, P.; Martins, J.R.R.A. Minimum lap time trajectory optimisation of performance vehicles with four-wheel drive and active aerodynamic control. *Veh. Syst. Dyn.* **2022**, 1–17. [CrossRef]

14.   Mashrouteh, S.; Khajepour, A.; Kasaiezadeh, A.; Esmailzadeh, E.; Chen, S.K.; Litkouhi, B. Multi-Actuation Controller for Performance Vehicles: Optimal Torque Allocation and Active Aerodynamic. *IEEE Trans. Veh. Technol.* **2022**, *71*, 2721–2733. [CrossRef]

15.   Shahein, A.H.; Ata, A.A.; Haraz, E.H.; El-Souhily, B.M. Vibration suppression of terrains irregularities using active aerodynamic surface for half-car model sport vehicles. *J. Vib. Control* **2020**, *26*, 2148–2162. [CrossRef]

16.   Muralidharan, V.; Balakrishnan, A.; Vardhan, V.K.; Meena, N.; Kumar, Y.S. Design of Mechanically Actuated Aerodynamic Braking System on a Formula Student Race Car. *J. Inst. Eng. Ser. C* **2018**, *99*, 247–253. [CrossRef]

17.   Devanuri, J.K. Numerical Investigation of Aerodynamic Braking for a Ground Vehicle. *J. Inst. Eng. Ser. C* **2018**, *99*, 329–337. [CrossRef]

18.   Nakashima, T.; Yan, C.; Moriuchi, T.; Kohri, I.; Mutsuda, H.; Doi, Y. Active aerodynamics control of simplified vehicle body in a crosswind condition. *J. Eng.* **2020**, *2020*, 1005–1011. [CrossRef]

19.   Piechna, J.R.; Kurec, K.; Broniszewski, J.; Remer, M.; Piechna, A.; Kamieniecki, K.; Bibik, P. Influence of the Car Movable Aerodynamic Elements on Fast Road Car Cornering. *Energies* **2022**, *15*, 689. [CrossRef]

20.   Szudarek, M.; Kamieniecki, K.; Tudruj, S.; Piechna, J. Towards Balanced Aerodynamic Axle Loading of a Car with Covered Wheels—Inflatable Splitter. *Energies* **2022**, *15*, 5543. [CrossRef]

21.   Kurec, K.; Remer, M.; Mayer, T.; Tudruj, S.; Piechna, J. Flow control for a car-mounted rear wing. *Int. J. Mech. Sci.* **2019**, *152*, 384–399. [CrossRef]

22.   Mathur, A.; Mahajan, A.; Aggarwal, A.; Mishra, C.; Roy, A. Numerical study of swan neck rear wing for enhancing stability of ground vehicle bodies. In Proceedings of the Lecture Notes in Mechanical Engineering; Springer Science and Business Media Deutschland GmbH: Berlin, Germany, 2021; pp. 199–208.

23.   Haunstetter, F. *Karosserie-Technikhighlights des Porsche 918 Spyder*; Springer Fachmedien: Wiesbaden, Germany, 2014; pp. 193–206.

24.   Lange, G.L. External Aerodynamic Optimization of Ground Vehicles Using the Adjoint Method. 2020. Available online: https://odr.chalmers.se/handle/20.500.12380/302243 (accessed on 5 September 2022).

25.   *ANSYS Fluent Theory Guide*; ANSYS, Inc.: Canonsburg, PA, USA, 2017; Volume 18.

26.   Menter, F.R. Two-equation eddy-viscosity turbulence models for engineering applications. *AIAA J.* **1994**, *32*, 1598–1605. [CrossRef]

27.   Zhang, C.; Bounds, C.P.; Foster, L.; Uddin, M. Turbulence Modeling Effects on the CFD Predictions of Flow over a Detailed Full-Scale Sedan Vehicle. *Fluids* **2019**, *4*, 148. [CrossRef]

28.   Kurec, K.; Remer, M.; Broniszewski, J.; Bibik, P.; Tudruj, S.; Piechna, J. Advanced Modeling and Simulation of Vehicle Active Aerodynamic Safety. *J. Adv. Transp.* **2019**, *2019*, 7308590. [CrossRef]

29.   Bugatii Veyron 16.4 Super Sport—Technical Specifications. Available online: https://assets.bugatti.com/fileadmin/media/Media/Veyron/Super_Sport/Technical_Specifications_Bugatti_Veyron_16.4_Super_Sport.pdf. (accessed on 29 June 2022).

30.   Lee, S.W.; Kim, H.L. Numerical Study of Active Aerodynamic Control via Flow Discharge on a High-Camber Rear Spoiler of a Road Vehicle. *Appl. Sci.* **2019**, *9*, 4783. [CrossRef]

31.   Kaushik, A.U.; Rao, N. Aerodynamic Optimization of Pylons to Improve Rear Wing Performance Using Passive and Active Systems. Master's Thesis, Chalmers University of Technology, Gothenburg, Sweden, 2020.

32.   Piechna, J.; Kurec, K.; Remer, M.; Kozar, M.; Popławski, J. PL239050B1—Układ do Tłumienia Drgań Nadwozia Pojazdu w Czasie Szybkiej Jazdy i Tylny Płat Dociskowy z Aktywnymi Elementami Aerodynamicznymi. Available online: https://odr.chalmers.se/handle/20.500.12380/302800 (accessed on 12 September 2022).

33.   Li, J.; Deng, Y.; Wang, Y.; Su, C.; Liu, X. CFD-Based research on control strategy of the opening of Active Grille Shutter on automobile. *Case Stud. Therm. Eng.* **2018**, *12*, 390–395. [CrossRef]

34.   Kurec, K.; Remer, M.; Piechna, J. The influence of different aerodynamic setups on enhancing a sports car's braking. *Int. J. Mech. Sci.* **2019**, *164*, 105140. [CrossRef]

35. Kurec, K.; Kamieniecki, K.; Piechna, J. Influence of Different Plates Arrangements on the Car Body. *Energies* **2022**, *15*, 619. [CrossRef]
36. Bugatti Chiron Sport—Technical Specifications. Available online: https://newsroom.bugatti/models/specifications/chironsport/180724_technical_specifications_bugatti_chiron_sport.pdf (accessed on 24 March 2019).